Acta Biomaterialia 74 (2018) 302–311

Contents lists available at ScienceDirect

Acta Biomaterialia

journal homepage: www.elsevier.com/locate/actabiomat

Full length article

Injectable magnetic supramolecular hydrogel with magnetocaloric liquid-conformal property prevents post-operative recurrence in a breast cancer model

Haoan Wu [a], Lina Song [b], Ling Chen [a], Wei Zhang [c], Yi Chen [a], Fengchao Zang [d], Hong Chen [e], Ming Ma [a], Ning Gu [a,*], Yu Zhang [a,*]

[a] State Key Laboratory of Bioelectronics, Jiangsu Key Laboratory for Biomaterials and Devices, School of Biological Science and Medical Engineering & Collaborative Innovation Center of Suzhou Nano Science and Technology, Southeast University, Nanjing 210096, PR China
[b] Department of Radiology, Affiliated Hospital of Nanjing University of Chinese Medicine, Nanjing 210029, PR China
[c] The Jiangsu Province Research Institute for Clinical Medicine, The First Affiliated Hospital with Nanjing Medical University, Nanjing 210029, PR China
[d] Jiangsu Key Laboratory of Molecular and Functional Imaging, Medical School, Southeast University, Nanjing 210009, PR China
[e] Department of Gastroenterology, Zhongda Hospital, School of Medicine, Southeast University, Nanjing 210009, PR China

ARTICLE INFO

Article history:
Received 20 January 2018
Received in revised form 25 April 2018
Accepted 26 April 2018
Available online 3 May 2018

Keywords:
Magnetic nanoparticles
Supramolecular hydrogel
Thermo-chemotherapy
Locoregional recurrence
Breast cancer

ABSTRACT

Locoregional recurrence of breast cancer after tumor resection represents several clinical challenges. Here, we demonstrate that co-delivery of chemotherapy and thermotherapeutic agents by a magnetic supramolecular hydrogel (MSH) following tumor resection prevents tumor recurrence in a breast cancer mouse model. The self-assembled MSH was designed through the partial inclusion complexation associated with the threading of α-CD on the copolymer moieties on the surface of the PEGylated iron oxide (Fe_3O_4) nanoparticles, which enables shear-thinning injection and controllable thermoreversible gel-sol transition. MSH was injected to the postoperative wound uniformly, which became mobile and perfect match with irregular cavity without blind angle due to the magnetocaloric gel-sol transition when exposed to alternating current magnetic field (ACMF). The magnetic nanoparticle-mediated induction heat during the gel-sol transition process caused the triggered release of dual-encapsulated chemotherapeutic drugs and provided an effect of thermally induced cell damage. The hierarchical structure of the MSH ensured that both hydrophobic and hydrophilic drugs can be loaded and consecutively delivered with different release curves. The hydrogel nanocomposite might provide a potential locally therapeutic approach for the precise treatment of locoregional recurrence of cancer.

Statement of Significance

Tumor recurrence after resection represents several clinical challenges. In this study, we prepared shear-thinning injectable magnetic supramolecular hydrogel (MSH) and demonstrated their therapeutic applications in preventing the post-operative recurrence of breast cancer with facile synthesis and minimally invasive implantation in vivo. MSH was injected to the postoperative wound uniformly, which become mobile and perfect match with irregular cavity without blind angle through magnetocaloric gel-sol transition when exposed to ACMF. The magnetic nanoparticles mediated induction heat during the gel-sol transition process caused the triggered release of dual-encapsulated chemotherapeutic drugs as well as thermally induced cell damage. This study demonstrates that MSH with the controlled administration of combined thermo-chemotherapy exhibit great superiority in terms of preventing post-operation cancer relapse.

1. Introduction

Cancer is still the leading cause of death around the world, with over 10 million new cases will be diagnosed each year. Breast can-

* Corresponding authors at: State Key Laboratory of Bioelectronics, Jiangsu Key Laboratory for Biomaterials and Devices, School of Biological Science and Medical Engineering, Southeast University, 87 Dingjiaqiao, District Gulou, Nanjing 210009, PR China.
E-mail addresses: guning@seu.edu.cn (N. Gu), zhangyu@seu.edu.cn (Y. Zhang).

https://doi.org/10.1016/j.actbio.2018.04.052
1742-7061/

cer remains the most widely cancer among women worldwide [1,2]. Surgical resection of the tumor is usually preferred in treatment for the majority of early breast cancer, the purpose of surgical resection is to remove as much of the tumor tissue as possible. However, the possible risk of recurrence from residual malignant cells remains high, especially in patients who have gone through the breast-conserving therapy [3]. The 10-year incidence rate of locoregional recurrence of breast cancer with stage I and II after therapy in women is 4–18%. Surgical resection of post-operative recurrence is difficult to implement and alternative rescue therapies are usually unsatisfactory. Moreover, progression of locoregional recurrences may eventually lead to great physical and mental suffering for the subsequent ulceration with odor, pain and bleeding [4,5].

Conventional surgery can hardly remove all the tumor cells and the peripheral infiltrating part, thus an inevitable recurrence always results in death. For the breast cancer, surgical resection of the primary tumor followed by systemic delivery of anticancer agents and localized radiotherapy to the breast is the standard clinical cure [6]. However, administration of systemic chemotherapy faces multiple challenges due to the low solubility, high side effects and short blood circulation of chemotherapeutic drugs [7,8]. Moreover, radiation injury to adjacent normal tissues, complicated procedures of radiation seeds to the surgical site, and concerns about wound repair have limited widely use of local radiotherapy [9]. Therefore, there is an urgent need for the development of more effective postoperatively adjuvant therapy that would improved efficacy with minimal side effects.

Local chemotherapy following tumour resection showed great application potential in treating the residual tumor cells. Localized drug delivery contains the implementation of implantable or injectable systems with targeted bioactive agents release characteristics that would destroy surviving malignant cells after resection and avoid the systemic side effects of chemotherapy via intravenous administration [10,11]. Various types of polymer-based chemotherapy delivery systems have been assessed as controlled release cargo for locoregional recurrence in several different malignancies. The Gliadel Wafer is the representative drug delivery implant for the clearance of postoperative brain tumor. In practice, several wafers are deposited along the surgical cavity following primary tumour resection [12]; Paclimer microspheres were used to prevent the recurrent ovarian cancer via intraperitoneal administration [13]; Numerous environmental responsive polyethylene glycol-based systems were applied to controlled drug delivery [14,15]. Nevertheless, most local drug delivery platforms cannot achieve an accurate match with irregular cavity, which always ignore the hollow and margin of the surgical cavity, thus resulting in uneven distribution of drugs and inhibiting the performance of the implant. At the same time, the single treatment form and the resistance to biodegradation of high molecular weight polymers also restrict their applications.

Cyclodextrins (CDs) are a series of cyclic oligosaccharides derived from starch, which have been widely used in biomedical applications for multiple purposes, primarily as a result of their extremely less toxicity, excellent biocompatibility and good solubilization ability with a range of hydrophobic drug molecules for delivery as well as their capability to form crystalline inclusion complex (IC) with poly(ethylene glycol) (PEG) [16,17]. Herein, we present the design of a novel magnetic supramolecular hydrogel (MSH) self-assembled by PEGylated iron oxide (Fe_3O_4) nanoparticles and α-CD through inclusion complexation for the locoregional recurrence of cancer following primary tumor resection in a breast mouse model. A biocompatible PEG-phospholipid (DSPE-MPEG2000) with amphiphilic character was used as the stabilizing agent in the preparation of PEGylated Fe_3O_4 nanoparticles, in which the DSPE block forms the shell around the magnetic core, while the MPEG block played as the guest molecule for the crystalline inclusion complex with a cyclic oligosaccharide host molecule, α-CD. The MSH composite of hierarchical structure contained both hydrophilic and hydrophobic domains, which enables dual loading of a hydrophobic molecule paclitaxel (PTX) into the shell structure of PEGylated Fe_3O_4 nanoparticles and another hydrophilic molecule Doxorubicin (DOX) into the aqueous bulk of the gel. Furthermore, drug release from MSH can be accelerated due to the magnetically induced heating of Fe_3O_4 nanoparticles under alternating current magnetic field (ACMF) irradiation. The MSH can be easily injected to the surgical residual position through a needle due to its shear-thinning property and liquid-conformally cover any residual cancerous cells on the margins or in the hollow of the cavity as it presents a magnetocaloric gel-sol transition when exposed to ACMF. Magnetically induced heating effect during the gel-sol transition procedure also affords tumor hyperthermia treatment simultaneously (Scheme 1).

2. Materials and methods

2.1. Materials

Iron(III) acetylacetonate [$Fe(acac)_3$ (98%)], Oleic acid ($C_{17}H_{33}$-COOH, 85%) and α-Cyclodextrin ($C_{36}H_{60}O_{30}$, 98%) were purchased from Aladdin Chemical Reagent Co., Ltd. Benzyl ether (98%) was purchased from Alfa Aesar. DSPE-MPEG2000 (PEG-phospholipids, 99%) was purchased from Shanghai A.V.T. Pharmaceutical Co., Ltd. Paclitaxel ($C_{47}H_{51}NO_{14}$, 98%) and DOX ($C_{27}H_{29}NO_{11}$·HCl, 98%) were purchased from Shanghai Yuanye Biotech Co., Ltd. Cy7 was purchased from Nanjing Nanoeast Biotech Co., Ltd. Gellan gum was purchased from Sigma Aldrich. The commercially available reagents, including Chloroform (98%), ethanol (95%), sodium propionate (CH_3CH_2COONa), 1,2-propanediol, were all purchased from Sinopharm Chemical Reagent Co., Ltd. All the chemicals were used as obtained without any further purification.

2.2. Oleic acid (OA)-coated Fe_3O_4 nanoparticles synthesis

The OA-coated Fe_3O_4 nanoparticles were successfully synthesized via a thermal decomposition procedure. In a typical reaction, 7.01 g (20 mmol) of $Fe(acac)_3$ and 20 mL (60 mmol) of OA were mixed in 100 mL of benzyl ether in a 500 mL three-neck flask. Under a nitrogen flow, the mixture was first heated to 220 °C. The solution was kept at this temperature for 60 min. Then the temperature was raised to 290 °C at a heating rate of 3 °C min^{-1} and kept at 290 °C for 45 min. The final solution was cooled to room temperature by removing the heating source. At last, the solution was precipitated by adding 50 mL of ethanol through magnetic separation, the precipitates were rewashed by 50 mL of ethanol for three times and dispersed in Chloroform.

2.3. Preparation of PEGylated Fe_3O_4 nanoparticles

As a typical example, DSPE-MPEG2000, PTX and Cy7 were all dissolved in 3 mL chloroform. OA-capped Fe_3O_4 MNPs (dispersed in 1 mL chloroform) and the above chloroform solution were mixed in a 50 mL round-bottom flask containing 3 mL of deionized water. Then, the reaction mixture was heated to 60 °C and chloroform was completely vaporized by slow evaporation for 15 min. After that, the Fe_3O_4 nanoparticles became water soluble.

2.4. Preparation of MSH

The general protocol for the hydrogel preparation is as follows. The aqueous solution of PEGylated Fe_3O_4 nanoparticles with differ-

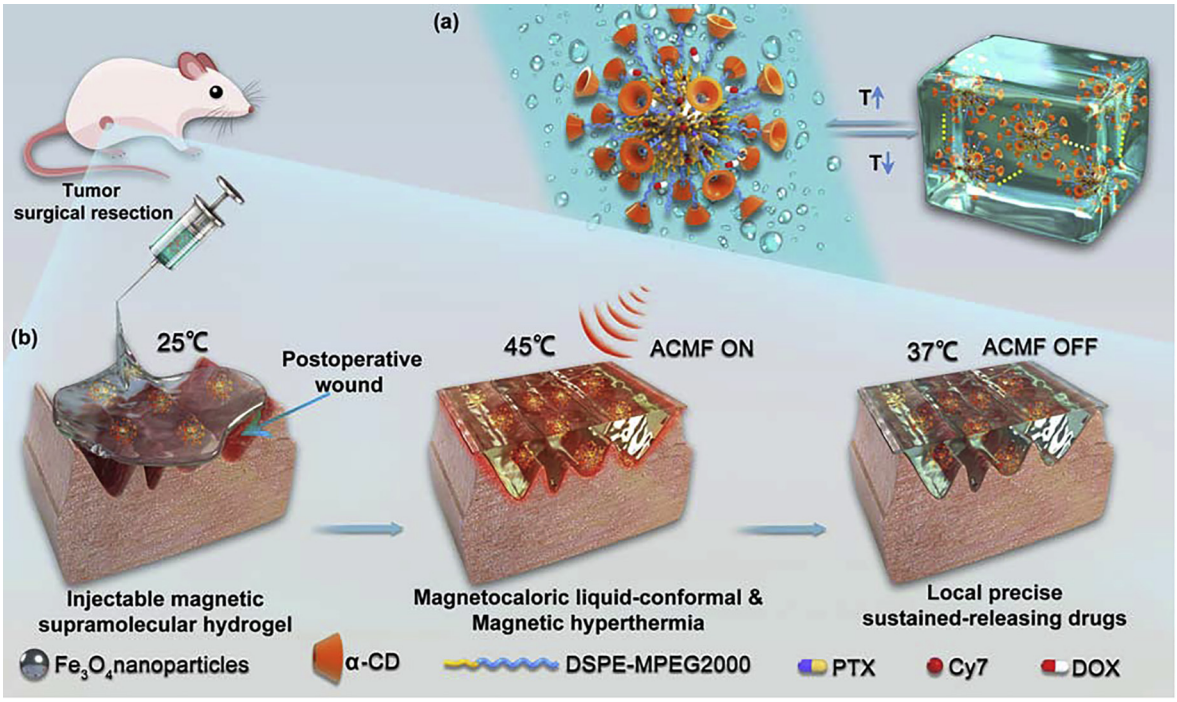

Scheme 1. Schematic illustration for the microstructure and application of MSH. (a) Temperature induced reversible gel-sol transition of MSH. (b) Magnetocaloric liquid-conformal at the tumor surgical resection site and the cancer thermo-chemotherapy.

ent DSPE-MPEG2000 concentrations (20% and 25%, w/v) was added to α-CD aqueous solutions (15%, 20%, and 30%, w/v) in equal volumes at room temperature. The solution was mixed uniformly through vortex mixer. The final concentration of iron in all hydrogel systems is 3 mg mL^{-1} and the concentration of DSPE-MPEG2000 is adjustable (20–25%, w/v). Various concentrations and different molar ratios of the DSPE-MPEG2000 to α-CD were taken to prepare hydrogels which have different gel-sol transition temperature (Tgel-s in the following).

2.5. Preparation of gellan gum-based tissue-mimicking gel and magnetic gellan gum hydrogel (MGH)

Gellan gum (2.5%, w/v), sodium (0.25%, w/v) and 1,2-propanediol propionate (20%, v/v) were dissolved in the deionized water under continuous stirring for 15 min at 90 °C. After that, the sample was sonicated in hot water for three minutes until the bubbles were removed from the solution, and then cooled into gel at 25 °C. Subsequently, the desired pattern was designed on the gel carefully with a knife. For the formation of MGH, the aqueous solution of PEGylated Fe_3O_4 nanoparticles was used as the water phase to make the gel. In addition, the final concentration of iron is 3 mg mL^{-1}, which is in agreement with the MSH.

2.6. Materials characterization

The morphology of the nanoparticles was observed by JEM-2100 electron microscope (JEOL) with a working voltage of 200 kV. Transmission electron microscopy (TEM) image of PEGylated Fe_3O_4 nanoparticles was taken from negatively stained by 2% sodium phosphotungstate (PH = 6.7). The M-H curves and magnetism of OA-coated Fe_3O_4 nanoparticles were obtained by a vibrating sample magnetometer (VSM, Lakeshore VSM 7407). Morphologies and element component of the MSH samples were studied by scanning electron microscopy (SEM, Ultra Plus, Carl Zeiss, Germany) after freeze-drying. Hydrodynamic size of the PEGylated Fe_3O_4 nanoparticles and the sol of MSH obtained by ACMF was analyzed by dynamic light scattering (DLS, Nano-ZS90, Malvern, England). X-ray diffraction (XRD) patterns of samples were detected at room temperature by an automatic X-ray diffractometer (X'TRA, ARL, Switzerland) using CuKα radiation.

2.7. Rheological experiments

Rheological properties were performed on a Physica MCR 302 (Anton Paar, Germany) equipped with coaxial cylinder geometry (PP25). Viscosity change at specific temperature was carried out by rotating speed over a range of 20–100 s^{-1} at a strain amplitude of γ = 1%.

The storage modulus (G′) and loss modulus (G″) of the hydrogel sample were tested at 25, 37 and 45 °C in oscillatory mode at a frequency of f = 1 Hz and strain amplitude of γ = 1%. Rheological experiments with oscillatory frequency sweeps at different temperatures and oscillatory temperature sweeps were also tested. Temperature-ramp experiments were carried out to monitor the viscoelastic moduli by heating the sample at a rate of 1 °C min^{-1} under the rotating speed of 50 s^{-1} at controlled regular strain amplitude of γ = 1%.

2.8. In vitro drug release

In vitro release studies were performed in a dialysis bag (molecular weight cutoff, 3.5 kDa) in 100 mL PBS with gentle shaking. In the collected fractions, PTX concentrations in the PBS 0.5% Tween 80 were investigated by a high performance liquid chromatography instrument (LC-20AT, Shimadzu). The analysis was monitored at 227 nm through a C18 column (Grace Analysis column) with the flow rate of mobile phase of acetonitrile/water/methanol (48:41:11 v/v) at 0.5 mL min^{-1}. The released DOX content can be detected by a UV spectrophotometer (UV-2401PC/2501PC, Shimadzu) at a wavelength of 254 nm according to the calibration curve of DOX.

2.9. In vitro heat induction measurements

The heat generation of PEGylated Fe_3O_4 nanoparticles and MSH in vitro was measured by a moderate radio frequency heating machine (Shuangping SPG-06-II, China). The sample tube was placed in a water-cooled magnetic induction copper coil with a frequency f of 410 kHz and a magnetic field intensity of 1.8 kA m^{-1}. The solution volume is 1 mL and the mass of Fe is 3 mg. The heating test time is 120 s. Specific absorption rate (SAR) values can accurately determine the heating ability of MSH and PEGylated Fe_3O_4 nanoparticles when an ACMF is applied. The SAR value of the sample was calculated with the following equation: SAR = Cw (dT/dt) (ms/mFe), where dT/dt is the initial slope of the graph, Cw is the specific heat capacity of the sample solution (specific heat capacity of water is 4.18 kJ kg^{-1} K^{-1}), mFe is the mass of Fe in the medium and ms is the mass of the suspension [18].

2.10. Cytotoxicity assay of MSH

The sol of MSH without drugs was diluted using DMEM to obtain the dilutions with different concentrations. RAW264.7 cells and 4T1 cells were seeded in 96-well plate at a concentration of 2 $\times$ 10^4 cells mL^{-1} and treated with MSH dilutions (0, 10, 20, 40, 60 , 80, 100 μg [Fe] mL^{-1}). After 24 h, 10 μL CCK-8 was added to each well and incubated at 37 °C for 5 h, then the absorbance at 450 nm was measured using microplate reader (Infinite 200 PRO). CCK-8 assay was carried out to evaluate the cytotoxicity of MSH.

2.11. Animal protocol

All animal care and experimental procedures were approved and performed according to the Animal Management Rules of the Ministry of Health of the People's Republic of China and the Guidelines with the approval of the Animal Care Committee of Southeast University. Female BALB/c mice (4 weeks of age, 20–25 g in weight) were purchased from the Model Animal Research Center of Southeast University. To establish the experimental model of the breast tumor, 4T1 cells (2 $\times$ 10^6, in 150 μL serum free RPMI-1640 medium) were subcutaneously injected into the right hind flank of each mouse.

2.12. In vivo MRI imaging

When the tumor size reached ~300 mm^3 (two weeks after establishment of animal model), segmental tumor tissues were surgically removed and left behind the irregular postoperative wound. MSH and MGH were placed onto the uneven surface of the residual tumor. MRI was carried out at 7.0 T Micro-MRI (PharmaScan, Brukers, Germany) with a 35 mm birdcage coil and small animal-cradle. 4% isoflurane/air gas mixture was delivered through a nose cone to anesthetize the mice. During the experimental period, the mice body temperature was maintained by a circulating warm water (37 °C). T2-weighted images were acquired by a flash sequence and the parameters were as follows: repetition time (TR) = 400 ms, echo time (TE) = 8.0 ms, Flip Angle = 30°, number of excitations (NEX) = 1, matrix size = 256 $\times$ 256, field of view (FOV) = 35 mm $\times$ 35 mm, slice thickness = 1 mm. Signal intensities were measured in defined regions of interest (ROIs) with Image J software.

2.13. In vivo thermo-chemotherapy of postoperative tumors

After the surgery (day 1), MSH was locally administrated through a syringe at the original tumor site and performed liquid-conformal procedure under irradiation of the ACMF, after that, MSH exhibited long term drug releasing control. To demonstrate the superiority of the liquid-conformal therapy of MSH vector, the efficacy was compared with implanted locally with MGH, injected locally with PEGylated Fe_3O_4 nanoparticles aqueous solution, intravenously with PEGylated Fe_3O_4 nanoparticles aqueous solution and injected locally with saline alone (blank control). All magnetic-induced hyperthermia experiments in vivo were carried out by a moderate radio frequency heating machine (Shuangping SPG-06-II, China) with the same parameters to in vitro test. The mice were placed into a water-cooled magnetic induction copper coil, where the tumors were located properly in the region of the ACMF. The duration of the magnetic hyperthermia application is 5 min. The temperature measurements were taken using an infrared-thermograph (Fulke, Ti32, USA). Body weight, local recurrence, and survival rate of each mouse at different groups in the following days were evaluated.

2.14. In vivo degradation by NIRF imaging

To indirectly observe the degradation of hydrogel in vivo, MSH which contained Cy7 was injected to the postoperative wound. The mice were placed into the center of electromagnetic induction heating coil for 5 min magnetocaloric liquid-conformal treatment, then the mice were imaged by a Maestro in vivo imaging system (Perkin Elmer, IVIS Lumina XRMS Series III). The degradation was assessed at day 1, 3, 7, 10, 15 postoperation. The optical imaging parameters were as follows: a magnification of $\times$2, a wavelength of 710 nm and a NIR emission filter.

2.15. Ex vivo histological staining

After treatment, the tissues surrounding the hydrogel and primary organs from tumor-bearing mice in different groups for various periods were collected in 5% neutral buffered formalin at room temperature. Then the tissues were fixed by paraffin and sectioned at a thickness of 3–5 μm. Ferric ions and cell nucleus were stained successively by Prussian blue and nuclear fast red (PB&NFR) respectively, haematoxylin and eosin (H&E) staining slides were prepared and then observed by bright field microscopy.

2.16. Statistical analysis

Statistical analyses were performed using GraphPad Prism 6.0 for Windows (LaJolla, CA). The results are presented as the mean SD (standard deviation). Two-way ANOVA with the Tukey test was used to assess the significant differences, in which a P-value less than 0.05 was accepted.

3. Results and discussion

3.1. Synthesis and characterization of MSH

Initially, MSH was formed by mixing aqueous α-CD solution containing DOX and aqueous dispersions of PEGylated Fe_3O_4 nanoparticles under ambient conditions. Here, a gelation occurred to result in the formation of a 3D supramolecular network via the inclusion complexes formed by MPEG block and α-CD. All systems can form injectable hydrogels within several seconds or several minutes, depending on the feed concentration (DSPE-MPEG2000 concentrations (20% and 25%, w/v) was added to α-CD aqueous solutions (15%, 20%, and 30%, w/v)). More interestingly, the gel has writing characters to create desired patterns on the substrate extruded from a syringe owing to its shear-thinning property (Fig. 1a, Movie S1).

The as-synthesized PEGylated Fe_3O_4 nanoparticles composed of a lipid layer of 5 nm and a magnetic core of 35 nm were showed in

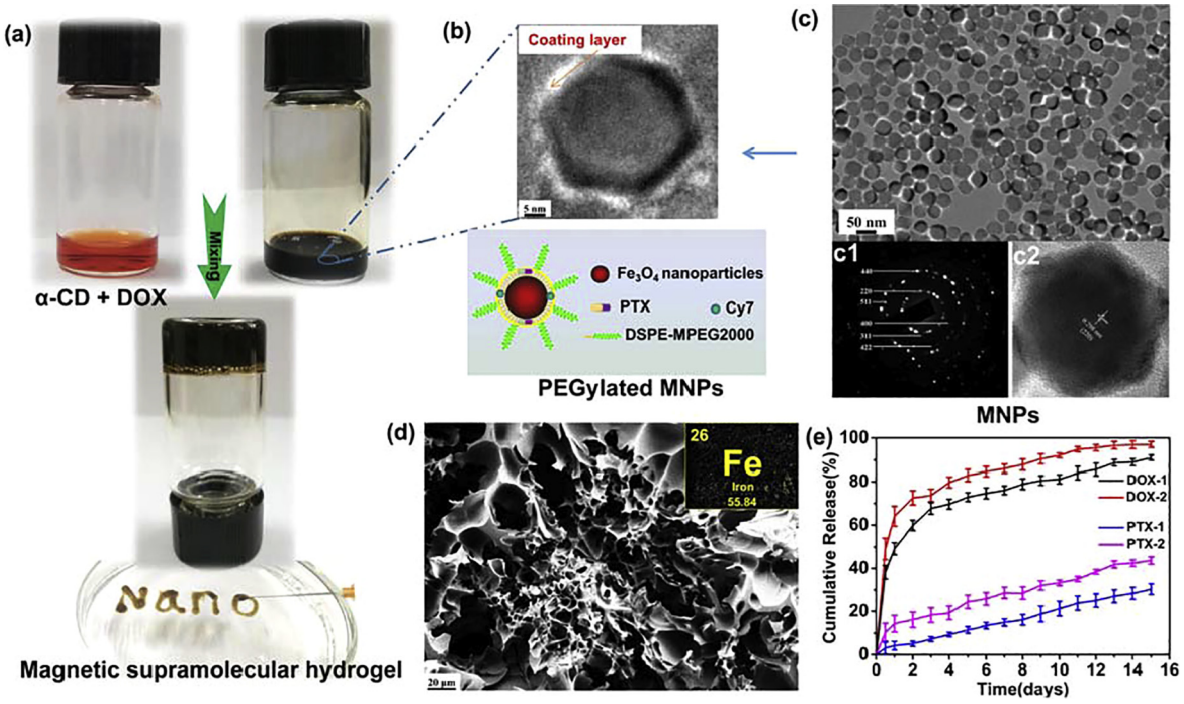

Fig. 1. (a) Formation of MSH composed of α-CD and PEGylated Fe_3O_4 MNPs. (b) Negatively stained TEM image and schematic diagram of the PEGylated MNPs, the red arrows point to the negative staining of the coating layer. (c) TEM image of MNPs, SAED pattern (c1) and HRTEM image (c2). (d) SEM image of freeze-dried MSH. Inset: the iron content embedded in the hydrogels can be better appreciated. (e) In vitro release curves for DOX and PTX of MSH with (2) or without (1) ACMF irradiation. (For interpretation of the references to colour in this figure legend, the reader is referred to the web version of this article.)

Fig. 1b. Fe_3O_4 nanoparticles with an average diameter of 35 nm [TEM image, Fig. 1c] were synthesized by a high temperature thermal decomposition procedure in the organic phase. The selective area electron diffraction [SAED, Fig. 1c1] patterns and HRTEM analysis (Fig. 1c2) indicate that the nanoparticles possess good crystallinity. A distinct DSPE-PEG2000 coating layer was visible in the negative stained TEM image, which encapsulated both antitumor drug PTX and near infrared fluorescent fat-soluble dye (Cy7).

After comparing three sizes of Fe_3O_4 nanoparticles, we choose nanoparticles with a mean particle diameter of around 35 nm for its high magnetically-induced heat generation efficiency and stability after PEG modification (Fig. S1). Magnetic measurements by VSM at 300 K demonstrated that the magnetic nanoparticles (MNPs) show a higher magnetization value [93.9 emu g^{-1} Fe, Fig. S2] compared to the commercial Ferumoxytol (56 emu g^{-1} Fe) [19]. From the SEM images, we can see that the morphology of the freeze-dried MSH showed a typical porous 3D network structure. The corresponding element mapping analysis of the hydrogel indicated the magnetic particle distribute uniformly throughout the hydrogel (Fig. 1d, Fig. S3). The formation of physical cross-links in the supramolecular polymer networks was further measured by XRD. As depicted in Fig. S4, it can be clearly observed that the pattern of MSH had a number of peaks and the main one at $2\theta = 19.7°$. It was due to the characteristic peak of the channel type structure of crystalline complex of MPEG/α-CD, suggesting that the inclusion complex of MPEG block and α-CD was the main driving force for the gelation of MSH [20,21].

Encapsulating multiple therapeutics simultaneously in a single material helps to reduce the number and dosage of medication as well as the resistance of tumors to single drugs. To determine the release kinetics of PTX and DOX from MSH, in vitro release studies were performed in a dialysis bag of 3.5 kDa in PBS containing 0.5% Tween 80 at 37.5 °C with gentle shaking. The incubation medium was replaced with fresh incubation solution at preset time points. Fig. 1e (DOX-1, PTX-1) shows the release profiles of the hydrogel and the loaded multiple therapeutics DOX and PTX could be released simultaneously. The two drugs showed dual independent release behaviors from MSH owing to the hierarchical structure of the gel, where the hydrophobic molecule PTX was wrapped into the lipid shell structure of nanoparticles and another hydrophilic molecule DOX was loaded into the aqueous bulk of the gel. We observed that the release rate of paclitaxel was low at 2% per day over the next 15 days and the MSH system released sustainedly only ~30% of PTX at half a month. The accumulated release percentage of DOX from hydrogel was about 60% in the first 2 days. The release was slow down after that and the total release percentage was more than 90% and the sustaining release time was half a month. For a better simulation of in vivo anti-cancer process, the release profile under ACMF irradiation was also investigated. The release of DOX and PTX from the MSH can be accelerated upon ACMF application. Samples were placed in our ACMF apparatus that maintains a baseline temperature of 37 °C and exposed for 5 min, the heat generated by PEGylated Fe_3O_4 nanoparticles raises the local temperature of the hydrogel, promoting increased drug diffusion through the hydrogel. Within 5 min after the ACMF irradiation, the cumulative amount of DOX release increased from 49 to 63% and 3 to 13% of PTX in the first day (Fig. 1e, DOX-2, PTX-2). Therefore, these intelligent hydrogels demonstrated an accelerative result, with the release of anticancer agents triggered with ACMF application.

3.2. Modulation of the magnetocaloric phase transition temperature of MSH

Since a large physical cross-linking force was provided with inclusion complexation structures which are easily affected by heat, the resulting MSH would experience a reversible gel-sol transition when heated to a temperature above the critical range named Tgel-s, different from a host of injectable hydrogels [22,23]. Fe_3O_4 nanoparticles exhibited a magnetically induced

heating phenomenon under irradiation of ACMF [24], therefore the resulting MSH displayed gel-sol transition under ACMF application with Fe_3O_4 nanoparticles as heat generators, resulted in a rise in temperature. Furthermore, the Tgel-s could be modulated by the concentration of DSPE-MPEG2000 and α-CD, as shown in thermal images of Fig. 2a, which was ascribed to an added aggregate force on account of the increasing number of crystalline micro-domains. In each case the MSH maintained its gel state adhered to the bottom of the bottle at 37 °C (refer to the dotted rectangle) and transformed to flowable solution within 3 min (indicated by the dotted oval) at different adjustable Tgel-s, and recovered to its solid state in 5 min in a 37 °C incubator. These observed results showed that the obtained MSH had fast magnetocaloric gel-sol transition under application of the ACMF. Moreover, there is no limit on the penetration depth of the ACMF making these MSHs more desirable than NIR light responsive materials. In the following experiments, we use the MSH with a Tgel-s of around 45 °C as the thermo-chemotherapy agent for its relative safety compared to higher temperature which was suitable for thermal ablation [25].

The mean hydrodynamic sizes (Number) of the PEGylated Fe_3O_4 nanoparticles were 63.5 nm and 64.1 nm in water and sol, which had the corresponding z-average sizes of 75 nm and 76.5 nm, respectively. Besides, the particle size distribution feature of MSH sol is nearly identical to that of the as-prepared PEGylated Fe_3O_4 nanoparticles (Fig. 2b). This result shows that the process of magnetocaloric reversible phase transition does not significantly alter the particle size distribution.

SAR value was usually used to evaluate the magnetic induction heat of MNPs in an ACMF. Magnetic induction heating capacity was closely connected with magnetic relaxation and the Ms value [26]. The MSH and PEGylated Fe_3O_4 nanoparticles with the same Fe content (3 mg mL^{-1}, 1 mL) induced temperature increase to ~100 °C under an ACMF (410 kHz, 1.8 kA m^{-1}) just for 80 s and revealed SAR values of 1334 and 1330 W g^{-1} Fe, respectively (Fig. 2c). MSH has the similar heating performance to PEGylated Fe_3O_4 nanoparticles, indicating that the resulting MSH network had no measurable impact on the relaxation of MNPs under the ACMF [27]. Such strong magnetic induction heating capacity of MSH is looking forward to be used in vivo magnetic hyperthermia of residual tumor cells. Furthermore, the mild mid-frequency ACMF we used has been proved to be harmless for potential biomedical application [28].

3.3. Liquid-adaptiveness of MSH under the magnetically induced heating

In the local adjuvant chemotherapy of cancer following primary tumor resection, locoregional recurrence is usually in relation to the drug-loaded hydrogel which cannot match the irregular shape of postoperative cavity [29]. Toward this purpose, we designed an intelligent local therapy hydrogel, which can be injected to the site of tumor resection with high target retention through the syringe, then matching the irregular cavity seamlessly by the magnetocaloric gel-sol transition under irradiation of the ACMF, and we called it "liquid-conformal". Subsequently, it will overspread any remaining cancer cells on the surface of the cavity and play therapeutic effect to cancerous cells to the utmost extent.

Firstly, we simulated the liquid-conformal process using the MSH which Tgel-s at 45 °C in vitro. The gellan gum-based tissue-mimic material which has thermal properties approximately equivalent to biological organ was used for the production of mould [30]. The mould has a center sag and branches out in eight different directions, where the MSH was injected into the sag and immobilized at 37 °C. MSH began to flow along the branch slowly when the temperature reached 45 °C under irradiation of the ACMF and filled in all the eight branches within 3 min (Movie S2). Afterwards, MSH returned to the solid state and attached to the base of mould when the temperature drops to 37 °C. As we can see from

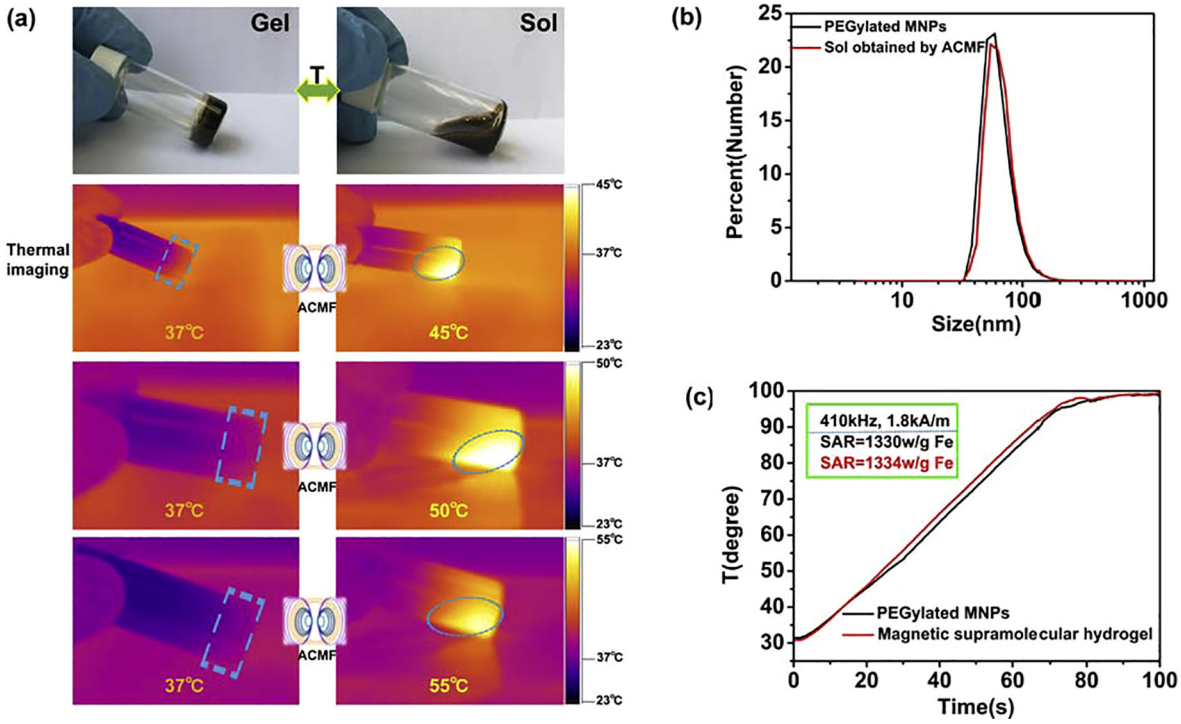

Fig. 2. (a) Digital photographs of temperature induced reversible gel-sol transition of MSH and the corresponding thermal images of MSH which has different gel-sol transition temperature (Tgel-s) under ACMF (Tgel-s = 45 °C: 20% DSPE-MPEG2000 (w/v) and 15% α-CD (w/v); Tgel-s = 50 °C: 20% DSPE-MPEG2000 (w/v) and 20% α-CD (w/v); Tgel-s = 55 °C: 25% DSPE-MPEG2000 (w/v) and 30% α-CD (w/v)). (b) DLS sizes measurement of PEGylated MNPs and sol of MSH obtained by ACMF. (c) Time-temperature curves of MSH and PEGylated MNPs in aqueous phase with the same concentration of 3 mg Fe mL^{-1} under ACMF (410 kHz, 1.8 kA m^{-1}).

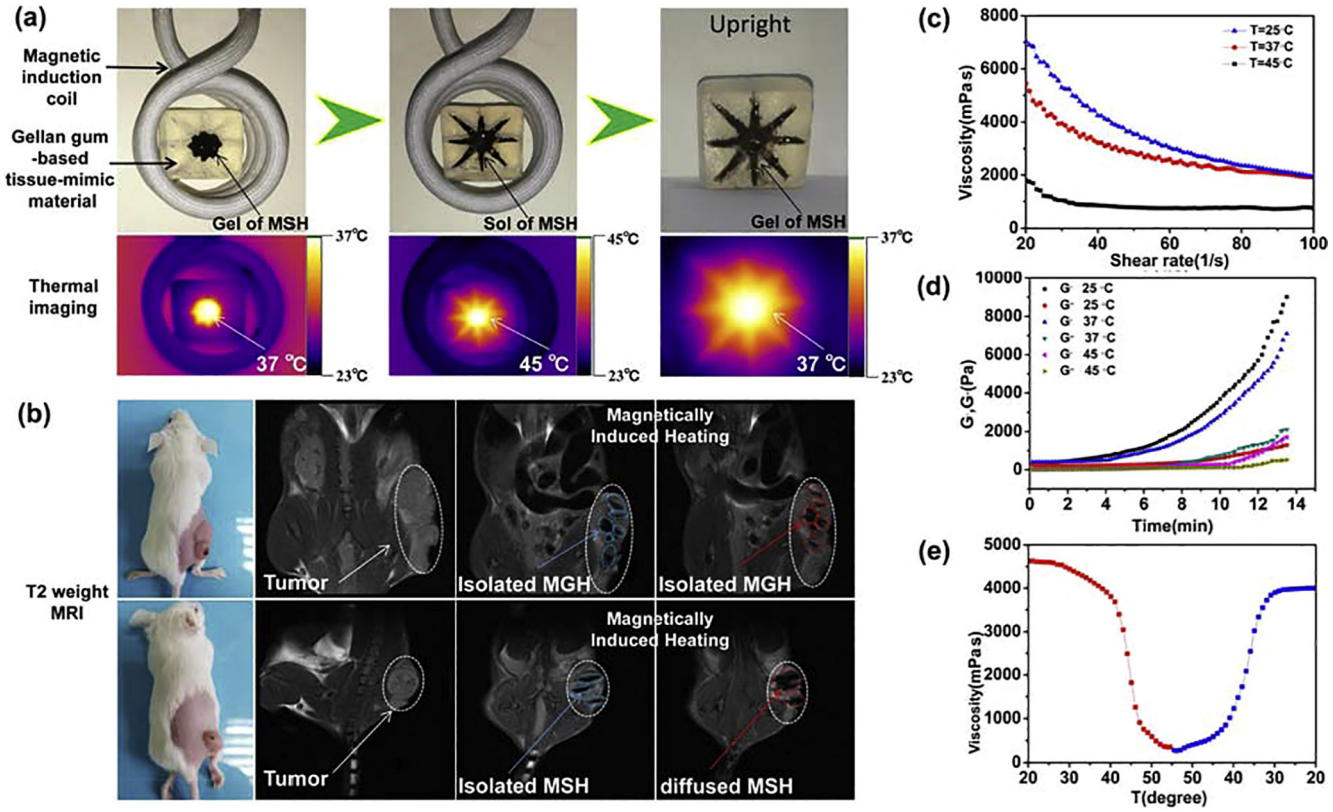

Fig. 3. (a) Magnetocaloric liquid-conformal of MSH on the gellan gum-based tissue-mimic material inside the copper coil under ACMF (410 kHz, 1.8 kA m^{-1}). (b) T2-weighted MR images of tumor-bearing mice following partial tumor resection acquired before and after injection of MSH or MGH and 5 min after exposure to ACMF (410 kHz, 1.8 kA m^{-1}). The white dashed circles indicated the tumor. Blue and red circles indicate hydrogels before and after ACMF irradiation respectively. (c) Viscosity change of the MSH at specific temperatures. (d) The time dependence of storage modulus (G′) and loss modulus (G″) for MSH at different temperatures. (e) The viscosity measurements of reversibility for MSH during temperature jumps. (For interpretation of the references to colour in this figure legend, the reader is referred to the web version of this article.)

Fig. 3a, the photographs and thermal images accurately reflect the variation of morphology as well as the temperature in real time of MSH during the liquid-conformal process.

To demonstrate the capacity of MSH for liquid-adaptiveness at irregular postoperative site in vivo, MRI was used to observe MSH state before and after magnetically induced heating and magnetic MGH with same concentration of Fe_3O_4 as a control. For this investigation, MSH and MGH were injected into residual tumor site after partial resection of orthotopic nodules in 4T1 tumor-bearing mice and subjected to MRI of T2-weighted pattern, permitting observation of hydrogels in situ tissue. These two injections were visualized both in the tissue coronal plane (Fig. 3b). We found that MGH injections were six isolated dark dots before and after magnetically induced heating, which were not influenced by the magnetic nanoparticle mediated temperature rises. By contrast, MSH injection sites began spreading out and merging with each other over the residual tumor hurdles between two injections under ACMF, demonstrating MSH had the ability to conformally fill the irregular postoperative tumor cavity. We also pay attention to the potential limitation of invasion of liquid MSH, that is the interstitial space, stromal spaces may also be invaded by the liquid formulation, leading to distant leakage. To avoid it, we will try to control the ACMF application time more precisely, insuring completely cover the wound but not easily spread beyond the postoperative area of the tumor.

Rheological experiments were carried out to analyze the gelation process and viscoelasticity of the MSH using small amplitude oscillatory shear. Fig. 3c displayed corresponding viscosities obtained at specific temperatures. The viscosity dramatically decreases with increasing shear rate (shear-thinning), which may be attributed to network dissociation and ease of injection. MSH developed to a tumor tissue implant in situ for its high viscosity and had high retention on the tumor site after surgical resection at room (25 °C) and physiological (37 °C) temperature. MSH with low viscosity upon the Tgel-s (45 °C) allowed for the liquid-conformal process during the magnetically induced heating under ACMF. The elastic and loss moduli G′ and G″ at different temperature were showed in Fig. 3d, which exhibited the characteristic viscoelastic behavior of gel at 25 °C and 37 °C, i.e., the values of G′ was observably larger than G″ over the time range investigated. While the value of G′ was near to G″ at Tgel-s (45 °C), indicating the properties of solvation, which can also be found in the oscillatory frequency sweeps at different temperatures (Fig. S5) and oscillatory temperature sweeps (Fig. S6). This may be attributed to the fact that a-CD could thread onto the MPEG polymer from both the ends resulting in the formation of physical cross-linked network and high temperature induced dissociation resulting from the disruption of physical cross-links. Fig. 3e shows the viscosities of MSH upon heating and cooling. During heating from 20 to 55 °C and subsequent cooling from 55 to 20 °C, the viscosities underwent a cycle variation of high-low–high values and recover more than 80% at 20 °C, demonstrating almost perfect thermoreversibility of the hydrogel. In addition, all the components of the MSH are biocompatible, relatively low cytotoxicity (Fig. S7) and can be quickly cleared off from the body, and the hydrogels show low shearing viscosity on account of the low molecular weight (∼2000) of polymer [31].

3.4. In vivo postoperative thermo-chemotherapy of MSH

Our main purpose was to develop a MSH-based vector with liquid-conformal ability for local tumor therapy, dual-therapeutic agent administration along with magnetic hyperthermia, which would collectively eliminate residual tumor cells and inhibit their recurrence following tumour resection.

The mice model of local tumor recurrence following resection of primary breast tumors was established to assess the local therapy efficiency of the MSH. The 4T1 cells (2×10^6) were subcutaneously injected into the right hind flank of female Balb/c mice to produce orthotopic primary tumors. When the tumor reached appropriately volume ($\sim$300 mm^3) 16–18 days after modeling, tumor resection surgery was carried out to mice after anesthetized by intraperitoneal injection of 6% chloral hydrate. The main tumor tissue was dissected away while 3%–5% volume of the tumors was preserved to undertake the recurrence in mice. All qualified mice were randomly assigned to five groups of 8–10 mice in each set and numbered.

After the surgery (day 1), MSH was locally administrated at the original point of tumor immediately (Fig. 4a) and performed liquid-conformal procedure by irradiation of the ACMF, where MSH went from isolated dots to a coherent hydrogel at 45 °C within 5 min and seamlessly matched with irregular residual tumor (Fig. S8, Movie S3). In the process of liquid-adaptiveness, MSH delivered dual-encapsulated chemotherapeutic drugs to kill remaining cancer cells following triggered release by ACMF irradiation, with accompanying tumor magnetic hyperthermia. For the next treatment, MSH exhibited sustained effective drug release over 15 days.

To allow noninvasively monitoring of the erosion course in vivo, near infrared fluorescent fat-soluble dye Cy7 was encapsulated in the lipid layer of PEGylated Fe_3O_4 nanoparticles. Fluorescent labeling has strong capacity in tracing erosion of hydrogel and delivery of bio-agents using an in vivo imaging system [32]. After injection, a visible gel developed beneath the skin, and a fairly high intensity was maintained for 15 days at the tumor site (Fig. 4b, c). As time proceeds, the brightness of fluorescence was gradually weakening, demonstrating that the hydrogels were constantly eroded. The residual MSH remained in the tumor site environment lasted for more than 4 weeks and, as a result, long-term therapy can be achieved (Fig. S9). This result indicated that MSH was maintained in the tumor region for a period of time and could be used as an injectable depot for sustained release of anticancer drugs.

Finally, the in vivo anticancer efficiency of MSH after a single magnetic hyperthermia and magnetocaloric liquid-conformal drug delivery under irradiation of the ACMF was assessed by monitoring the tumor local recurrence, body weight and survival rate within the treatment duration. After 1, 2, 3, and 4 weeks, 3 mice from each group were sacrificed, and the tissues surrounding the hydrogel were harvested, stained with H&E double staining as well as PB&NFR double staining, and then processed for histological examination to explore the mechanism of tumor regression (Fig. 5a). H&E staining indicated that the tumor cells and some inflammatory cells can be seen in the first two weeks while only muscular tissues was observed by the end of the fourth week. It proved that tumor cells were constantly being killed and the slight inflammatory reaction had disappeared after 4 weeks. As shown in the PB&NFR double staining, the blue stripe reflecting the MSH adhered to tumor border zone during the first two weeks . As time goes on, cancer cells continue to die until they disappear completely and a few blue dots which stand for MSH still can be found in the next two weeks for the long time release of anticancer drugs. Pathological analysis as a strong microscopic evidence to prove the good therapeutic effect of MSH by the introducing of ACMF. The wound of mice treated with MSH began to close up gradually and the scars tissue within the original wound boundary were totally healed after 4 weeks of feeding (Digital photos, Fig. 5a). Histological examination of main organs showed in Fig. S10 including heart, liver, spleen, lung and kidney of the four treatment groups 5 days post-injection showed that no abnormality occurred in these organs and did not reveal any changes in the physical architecture

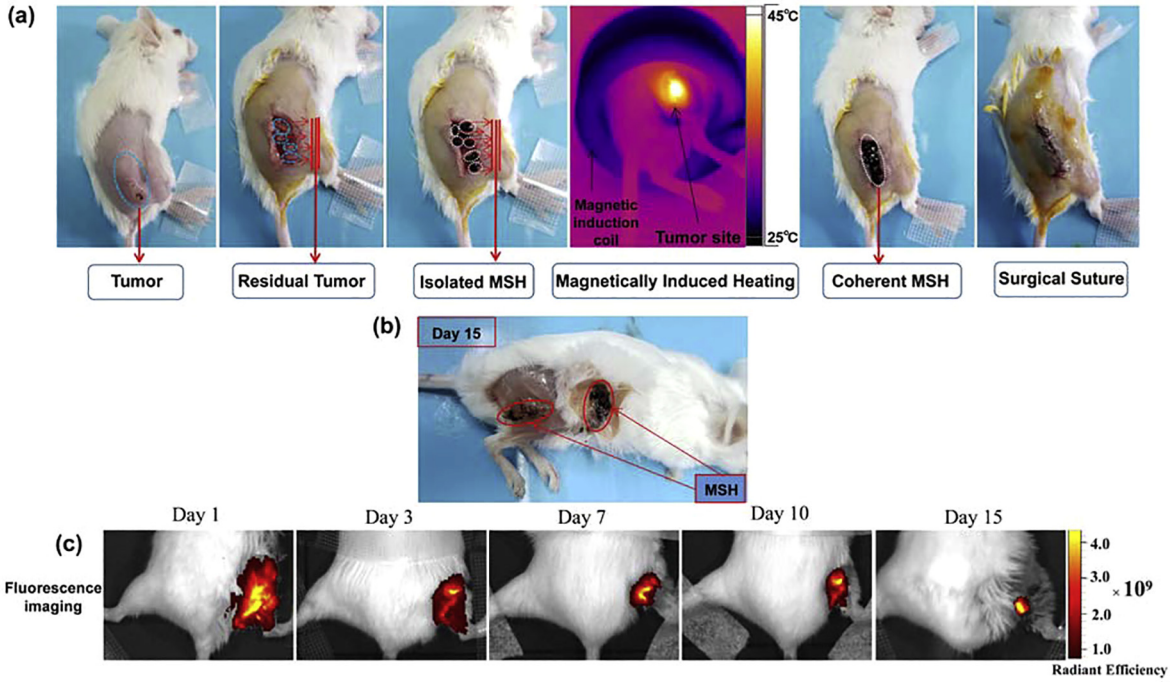

Fig. 4. (a) Live imaging of 4T1 tumor-bearing mice implanted with MSH that contained dual-drug and MNPs with liquid-conformal thermo-chemotherapy treatment after tumour resection. (b) The existence of the gel was checked after mice were sacrificed at day 15. (c) In vivo degradation behavior monitored by Near-IR fluorescence imaging over 15 days.

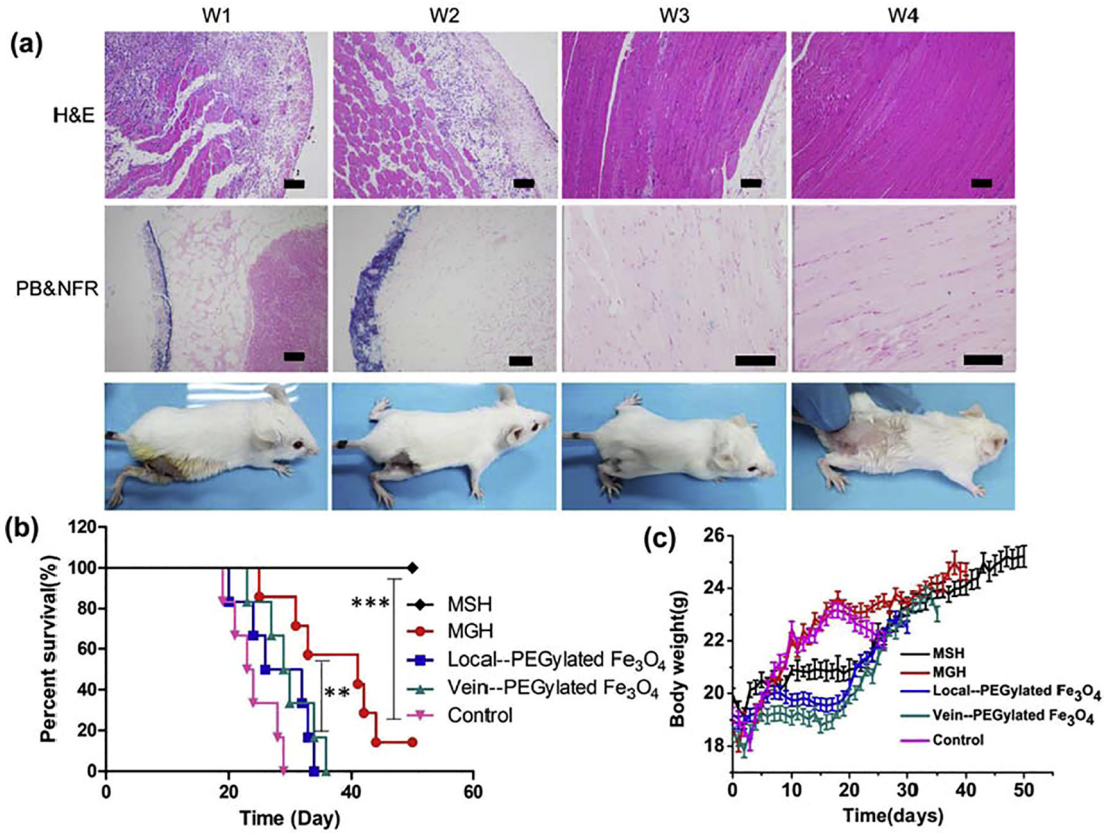

Fig. 5. (a) H&E staining and PB&NFR double staining images of tumor surrounding tissue sections harvested from 4T1 tumor-bearing mice treated with MSH for several time points (from 1 week to 4 weeks). Digital photos ($w_1 - w_4$) show the wound healing of MSH-implanted 4T1 tumor-bearing mice after single treatment for extended days. Scale bars, 100 μm. (b) The long-term survival rate of mice bearing 4T1 tumor after several treatment processes as indicated. (c) Body weight assessment was performed on all the animal groups after hydrogel implantation. Body weight depicted as the mean of each treatment group. Measurement for each treatment was repeated in triplicate, and the results were presented as mean SD (**, $P < 0.01$, ***, $P < 0.001$, $n = 8$).

of the organs in comparison to the blank control group. The longer term H&E staining analysis from the major organs of MSH group on different days (Fig. S11) revealed no obvious pathological tissue damage found in mice, further demonstrating that the well in vivo biocompatibility of MSH administrated subcutaneously.

To further display the meliority of the liquid-conformal therapy using MSH vector, the therapeutic efficacy of MSH was in comparison to locally implanted MGH, locally injected PEGylated Fe_3O_4 nanoparticles, intravenously injected PEGylated Fe_3O_4 nanoparticles, taking local injected saline as a blank control (Fig. S12). All material groups except blank control have the same concentration of Fe, PTX and DOX. The body weight, wound healing, evidence of local recurrence, and survival of mice were monitored every day for up to 50 days.

Survival study was performed for mice following MSH therapy or control therapies. Visible locoregional recurrences of post-operative were monitored in 20 days in mice locally administered with MGH (75%), mice that received PEGylated Fe_3O_4 nanoparticles local administration(83.5%), mice intravenously injected with PEGylated Fe_3O_4 nanoparticles (85%), and the whole mice in the blank control group (100%) (Fig. S13). In marked contrast, neither one of the 8 mice cured with MSH formed local recurrence at the site of the gel and had significantly survival advantage (Fig. 5b) (100% survival for at least 60 days). While, recurrence in other control groups was obviously deferred than the blank control and MGH is superior in restraining local tumor recurrence when compared with the same dose of drug for delivered systemically or locally administered PEGylated Fe_3O_4 nanoparticles solution. The mice receiving tumor resection all exhibited weight loss in the first 1–2 days of the treatments for the primary tumor volume is relatively large and the part of the tumor grows into leg muscle tissue, where the mice underwent surgery operation usually have a large impact on quality of life and weight. Afterwards, the mice treated locally with the MSH revealed steadily developed tumor weight, pointing at hydrogel biocompatibility (Fig. 5c). The therapy of MSH implanted following resection was capable of killing tumor cells and inhibiting the re-growth of tumor cells. There was still no direct evidence that shows tumor recurrence in the MSH group two months after tumour resection and the MSH therapy has obvious advantages in therapeutic effect compared with other therapies.

4. Conclusion

In summary, we prepared shear-thinning injectable magnetic hydrogels utilizing inclusion complexation between PEGylated Fe_3O_4 nanoparticles and α-CD, and demonstrated their therapeutic applications in eliminating the post-operative recurrence of breast tumor with mild synthesis and minimally invasive injection in vivo. MSH revealed magnetocaloric liquid-conformal ability to perfectly match the irregular cavity following tumor resection without blind angle when exposed to ACMF. Moreover, biocompatible supramolecular hydrogels enabled co loading of a hydrophobic molecule into the lipid layer of MNPs and another hydrophilic molecule into the massive construction of the gel. The dual structure of the MSH afforded different release processes of diverse drug molecular from an unitary sample and localized long-term delivery of anti-cancer drugs. The MNPs-mediated induction heat during

the gel-sol transition process caused the thermally induced cell damage and triggered release of chemotherapeutic drugs. MSH synergistically eliminates the tumor and prevents the local recurrence completely of breast cancer following surgically resection. This study demonstrates that MSH with the controlled administration of combined thermo-chemotherapy exhibit great superiority in terms of preventing post-operation cancer relapse.

Acknowledgements

This research was supported by the National Key Research and Development Program of China (No. 2017YFA0205502), the National Basic Research Program of China (973 program No. 2013CB733800), National Natural Science Foundation of China (Nos. 81571806, 81671820), the Jiangsu Provincial Special Program of Medical Science (BL2013029), and the Fundamental Research Funds for the Central Universities.

Appendix A. Supplementary data

Supplementary data associated with this article can be found, in the online version, at https://doi.org/10.1016/j.actbio.2018.04.052.

References

[1] J. Conde, N. Oliva, Y. Zhang, N. Artzi, Local triple-combination therapy results in tumour regression and prevents recurrence in a colon cancer model, Nat. Mater. 15 (2016) 1128.
[2] N. Lei, C. Gong, Z. Qian, F. Luo, C. Wang, H. Wang, Y. Wei, Therapeutic application of injectable thermosensitive hydrogel in preventing local breast cancer recurrence and improving incision wound healing in a mouse model, Nanoscale 4 (2012) 5686–5693.
[3] E. Ruel-Gariépy, M. Shive, A. Bichara, M. Berrada, G.D. Le, A. Chenite, J.C. Leroux, A thermosensitive chitosan-based hydrogel for the local delivery of paclitaxel, Eur. J. Pharm. Biopharm. 57 (2004) 53.
[4] Y. Qu, B.Y. Chu, J.R. Peng, J.F. Liao, T.T. Qi, K. Shi, X.N. Zhang, Y.Q. Wei, Z.Y. Qian, A biodegradable thermo-responsive hybrid hydrogel: therapeutic applications in preventing the post-operative recurrence of breast cancer, Npg Asia Mater. 7 (2015) e207.
[5] S. Maluta, M.W. Kolff, Role of hyperthermia in breast cancer locoregional recurrence: a review, Breast Care 10 (2015) 408–412.
[6] F.P. Seib, E.M. Pritchard, D.L. Kaplan, Self-assembling doxorubicin silk hydrogels for the focal treatment of primary breast cancer, Adv. Funct. Mater. 23 (2013) 58.
[7] M. Singh, S. Kundu, M.A. Reddy, V. Sreekanth, R.K. Motiani, S. Sengupta, A. Srivastava, A. Bajaj, Injectable small molecule hydrogel as a potential nanocarrier for localized and sustained in vivo delivery of doxorubicin, Nanoscale 6 (2014) 12849–12855.
[8] D.L. Liu, X. Chang, C.M. Dong, Reduction- and thermo-sensitive star polypeptide micelles and hydrogels for on-demand drug delivery, Chem. Commun. 49 (2013) 1229–1231.
[9] R. Liu, J.B. Wolinsky, J. Walpole, E. Southard, L.R. Chirieac, M.W. Grinstaff, Y.L. Colson, Prevention of local tumor recurrence following surgery using low-dose chemotherapeutic polymer films, Ann. Surg. Oncol. 17 (2010) 1203.
[10] S. Xu, L. Yin, Y. Xiang, H. Deng, L. Deng, H. Fan, H. Tang, J. Zhang, A. Dong, Supramolecular hydrogel from nanoparticles and cyclodextrins for local and sustained nanoparticle delivery, Macromol. Biosci. 16 (2016) 1188.
[11] C.B. Rodell, J.W. Macarthur, S.M. Dorsey, R.J. Wade, L.L. Wang, Y.J. Woo, J.A. Burdick, Shear-thinning supramolecular hydrogels with secondary autonomous covalent crosslinking to modulate viscoelastic properties in vivo, Adv. Funct. Mater. 25 (2015) 636.
[12] M.A. Moses, H. Brem, R. Langer, Advancing the field of drug delivery: taking aim at cancer, Cancer Cell 4 (2003) 337–341.
[13] J.B. Wolinsky, Y.L. Colson, M.W. Grinstaff, Local drug delivery strategies for cancer treatment: gels, nanoparticles, polymeric films, rods, and wafers, J. Control Release 159 (2012) 14.
[14] E.A. Appel, M.W. Tibbitt, M.J. Webber, B.A. Mattix, O. Veiseh, R. Langer, Self-assembled hydrogels utilizing polymer-nanoparticle interactions, Nat. Commun. 6 (2015) 6295.
[15] Y. Chen, X.H. Pang, C.M. Dong, Dual stimuli-responsive supramolecular polypeptide-based hydrogel and reverse micellar hydrogel mediated by host-guest chemistry, Adv. Funct. Mater. 20 (2010) 579–586.
[16] H. He, S. Chen, J. Zhou, Y. Dou, L. Song, L. Che, X. Zhou, X. Chen, Y. Jia, J. Zhang, S. Li, X. Li, Cyclodextrin-derived pH-responsive nanoparticles for delivery of paclitaxel, Biomaterials 34 (2013) 5344.
[17] Z. Zhang, Z. He, R. Liang, Y. Ma, W. Huang, R. Jiang, S. Shi, H. Chen, X. Li, Fabrication of a micellar supramolecular hydrogel for ocular drug delivery, Biomacromolecules 17 (2016) 798.
[18] S. Mornet, S. Vasseur, F. Grasset, E. Duguet, Magnetic nanoparticle design for medical diagnosis and therapy, J. Mater. Chem. 14 (2004) 2161–2175.
[19] B. Chen, Y. Li, X. Zhang, F. Liu, Y. Liu, M. Ji, F. Xiong, N. Gu, An efficient synthesis of ferumoxytol induced by alternating-current magnetic field, Mater. Lett. 170 (2016) 93–96.
[20] D. Ma, H.B. Zhang, K. Tu, L.M. Zhang, Novel supramolecular hydrogel/micelle composite for co-delivery of anticancer drug and growth factor, Soft Matter 8 (2012) 3665–3672.
[21] J. Li, X. Li, X. Ni, X. Wang, H. Li, K.W. Leong, Self-assembled supramolecular hydrogels formed by biodegradable PEO-PHB-PEO triblock copolymers and alpha-cyclodextrin for controlled drug delivery, Biomaterials 27 (2006) 4132–4140.
[22] R. Du, J. Wu, L. Chen, H. Huang, X. Zhang, J. Zhang, Hierarchical hydrogen bonds directed multi-functional carbon nanotube-based supramolecular hydrogels, Small 10 (2014) 1387–1393.
[23] D. Ma, L.M. Zhang, Fabrication and modulation of magnetically supramolecular hydrogels, J. Phys. Chem. B 112 (2008) 6315.
[24] N. Lee, D. Yoo, D. Ling, H.C. Mi, T. Hyeon, J. Cheon, Iron oxide based nanoparticles for multimodal imaging and magnetoresponsive therapy, Chem. Rev. 115 (2015) 10637.
[25] H. Wu, L. Song, L. Chen, Y. Huang, Y. Wu, F. Zang, Y. An, H. Lyu, M. Ma, J. Chen, N. Gu, Y. Zhang, Injectable thermosensitive magnetic nanoemulsion hydrogel for multimodal-imaging-guided accurate thermoablative cancer therapy, Nanoscale (2017).
[26] Y.W. Jun, J.H. Lee, J. Cheon, Chemical design of nanoparticle probes for high-performance magnetic resonance imaging, Cheminform 39 (2008) 5122–5135.
[27] J.P. Fortin, C. Wilhelm, J. Servais, C. Ménager, J.C. Bacri, F. Gazeau, Size-sorted anionic iron oxide nanomagnets as colloidal mediators for magnetic hyperthermia, J. Am. Chem. Soc. 129 (2007) 2628–2635.
[28] J. Xie, Y. Zhang, C. Yan, L. Song, S. Wen, F. Zang, G. Chen, Q. Ding, C. Yan, N. Gu, High-performance PEGylated Mn-Zn ferrite nanocrystals as a passive-targeted agent for magnetically induced cancer theranostics, Biomaterials 35 (2014) 9126.
[29] J. Tao, J. Zhang, Y. Hu, Y. Yang, Z. Gou, T. Du, J. Mao, M. Gou, A conformal hydrogel nanocomposite for local delivery of paclitaxel, J. Biomater. Sci. Polym. Ed. 28 (2016) 1.
[30] R.K. Chen, A.J. Shih, Multi-modality gellan gum-based tissue-mimicking phantom with targeted mechanical, electrical, and thermal properties, Phys. Med. Biol. 58 (2013) 5511–5525.
[31] S. Zhao, J. Lee, Supramolecular hydrogels instantaneously formed by inclusion complexation between amphiphilic oligomers and α-cyclodextrins, Macromol. Res. 17 (2009) 156–162.
[32] N. Artzi, N. Oliva, C. Puron, S. Shitreet, S. Artzi, A.B. Ramos, A. Groothuis, G. Sahagian, E.R. Edelman, In vivo and in vitro tracking of erosion in biodegradable materials using non-invasive fluorescence imaging, Nat. Mater. 10 (2011) 704–709.